

000
001
002054
055
056

External Prior Guided Internal Prior Learning for Real Noisy Image Denoising

057
058
059003
004
005
006
007
008
009
010
011060
061
062
063
064
065

Anonymous CVPR submission

012

066

013

067
068

Abstract

014

069

015

070
071

016

072
073

017

074
075

018

076
077

019

078
079

020

080
081
082

021

083
084
085

022

086
087
088

023

089
090
091

024

092
093

025

094
095
096

026

097
098
099

027

100
101
102

028

103
104
105

029

106
107

030

108
109
110

031

111
112
113

032

114
115
116

033

117
118
119

034

120
121
122

035

123
124
125

036

126
127
128

037

129
130
131

038

132
133
134

039

135
136
137

040

138
139
140

041

141
142
143

042

144
145
146

043

147
148
149

044

150
151
152

045

153
154
155

046

156
157
158

047

159
160
161

048

162
163
164

049

165
166
167

050

168
169
170

051

171
172
173

052

174
175
176

053

177
178
179

Paper ID 1047

External Prior Guided Internal Prior Learning for Real Noisy Image Denoising

Anonymous CVPR submission

Paper ID 1047

Abstract

Most of existing image denoising methods use some statistical models such as additive white Gaussian noise (AWGN) to model the noise, and learn image priors from either external data or the noisy image itself to remove noise. However, the noise in real-world noisy images is much more complex than AWGN, and it is hard to be modeled by simple analytical distributions. Therefore, many state-of-the-art denoising methods in literature become much less effective when applied to real noisy images. In this paper, we develop a robust denoiser for real noisy image denoising without explicit assumption on noise models. Specifically, we first learn external priors from a set of clean natural images, and then use the learned external priors to guide the learning of internal latent priors from the given noisy image. The proposed method is simple yet highly effective. Experiments on real noisy images demonstrate that it achieves much better denoising performance than state-of-the-art denoising methods, including those designed for real noisy images.

1. Introduction

Image denoising is a crucial and indispensable step to improve image quality in digital imaging systems. In particular, with the decrease of size of CMOS/CCD sensors, noise is more easily to be corrupted and hence denoising is becoming increasingly important for high resolution imaging. In literature of image denoising, the observed noisy image is usually modeled as $\mathbf{y} = \mathbf{x} + \mathbf{n}$, where \mathbf{x} is the latent clean image and \mathbf{n} is the corrupted noise. Numerous image denoising methods [1, 2, 3, 4, 5, 6, 7, 8, 9, 10, 11, 12, 13] have been proposed in the past decades, including sparse representation and dictionary learning based methods [1, 2, 3], nonlocal self-similarity based methods [4, 5, 6, 3, 7], low-rank based methods [8], neural network based methods [9], and discriminative learning based methods [10, 11].

Most of the existing denoising methods [1, 2, 4, 5, 6, 3, 7, 8, 9, 10, 11, 12, 13] mentioned above assume noise \mathbf{n} to be additive white Gaussian noise (AWGN). Unfortunately, this assumption is too ideal to be true for real-world noisy im-

ages, where the noise is much more complex than AWGN [14, 15] and varies by different cameras and camera settings (ISO, shutter speed, and aperture, etc.). According to [15], the noise corrupted in the imaging process [is signal dependent and comes from five main sources: photon shot, fixed pattern, dark current, readout, and quantization noise. As a result, many advanced denoising methods in literature becomes much less effective when applied to real-world noisy images. Fig. 1 shows an example, where we apply some representative and state-of-the-art denoising methods, including CBM3D [6], WNNM [8], MLP [9], CSF [10], and TRD [11], to a real noisy image (captured by a Nikon D800 camera with ISO is 3200) provided in [14]. One can see that these methods either remain the noise or over-smooth the image details on this real noisy image.

There have been a few methods [16, 17, 18, 14, 19, 20, 21] developed for real noisy image denoising. Almost all of these methods follow a two-stage framework: first estimate the parameters of the assumed noise model (usually Gaussian or mixture of Gaussians (MoG)), and then perform denoising with the estimated noise model. Again, the noise in real noisy images is very complex and hard to be modeled by explicit distributions such as Gaussian and MoG. Fig. 1 also shows the denoised results of two state-of-the-art real noisy image denoising methods, Noise Clinic [19, 20] and Neat Image [21]. One can see that these two methods do not perform well on this noisy image either.

This work aims to develop a robust solution for real noisy image denoising without explicitly assuming certain noise models. To achieve this goal, we propose to first learn image priors from external clean images, and then employ the learned external priors to guide the learning of internal latent priors from the given noisy image. The flowchart of the proposed method is illustrated in Fig. 2. We first extract millions of patch groups from a set of high quality natural images, with which a Gaussian Mixture Model (GMM) is learned as the external prior. The learned GMM prior model is used to cluster the patch groups extracted from the given noisy image, and then a hybrid orthogonal dictionary (HOD) is learned as the internal prior for image denoising. Our proposed denoising method is simple and ef-

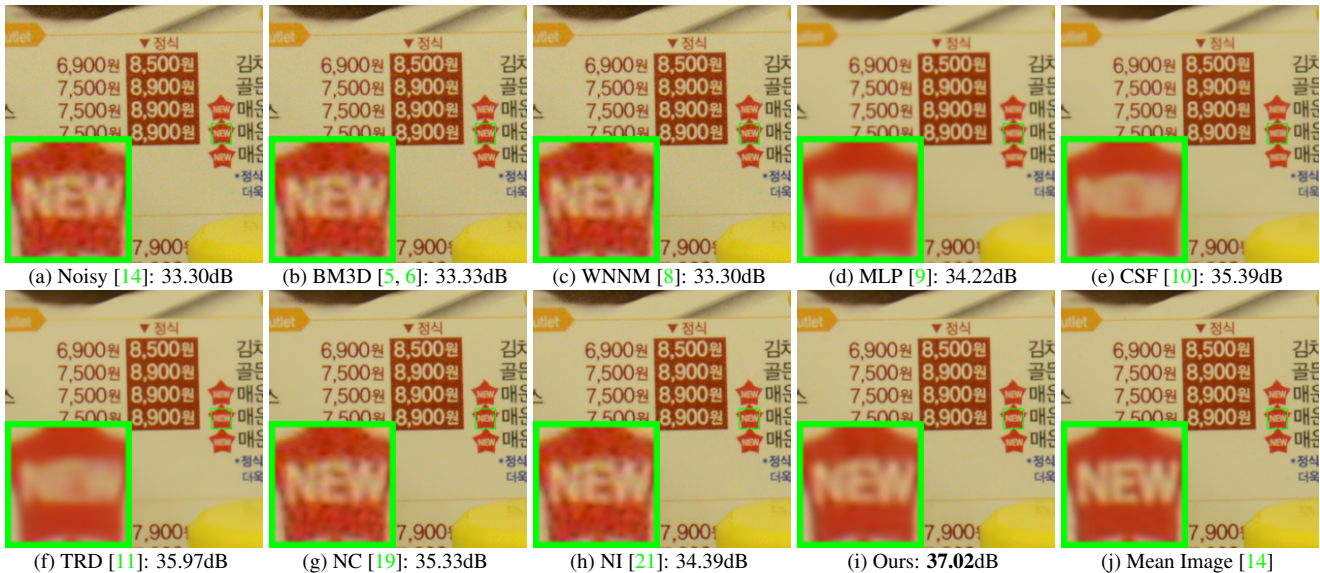


Figure 1. Denoised images of the real noisy image “Nikon D800 ISO 3200 A3” from [14] by different methods. The images are better viewed by zooming in on screen.

ficient, yet our extensive experiments on real noisy images clearly demonstrate its better denoising performance than the current state-of-the-arts.

2. Related Work

2.1. Internal vs. External Prior Learning

Image priors are playing a key role in image denoising [7, 13, 1, 22, 3, 23]. There are mainly two categories of prior learning methods. 1) External prior learning methods [12, 7, 13] learn priors (e.g., dictionaries) from a set of external clean images, and the learned priors are used to recover the latent clean image from noisy images. 2) Internal prior learning methods [1, 3, 22, 23] directly learn priors from the given noisy image, and the image denoising is often done simultaneously with the prior learning process. It has been demonstrated [7, 13] that the external priors learned from natural clean images are effective and efficient for image denoising problem, but they are not adaptive to the given noisy image so that some fine-scale image structures may not be well recovered. By contrast, the internal priors are adaptive to content of the given image, but the learning processing are usually slow. In addition, most of the internal prior learning methods [1, 3, 22, 23] assume AWGN noise, making the learned priors less robust for real noisy images. In this paper, we use external priors to guide the internal prior learning. Our method is not only much faster than the traditional internal learning methods, but also very effective to denoise real noisy images.

2.2. Real Noisy Image Denoising

Recently, several denoising methods [16, 17, 19, 20, 18, 14] are proposed to remove unknown noise in noisy images.

These methods can be directly applied to denoise real noisy images. Among them, the “Noise Clinic” [19, 20] estimated the noise by a multivariate Gaussian and remove the noise by a generalized version of nonlocal Bayesian model [24]. Zhu *et al.* proposed a Bayesian method [18] to approximate and remove the noise via a low-rank MoG model. There are also several methods developed specifically for real noisy image denoising [14, 21]. The [14] modeled the cross-channel noise in real noisy image as a multivariate Gaussian and the noise is removed by Bayesian nonlocal means. The commercial software Neat Image [21] estimated the noise parameters from a flat region of the given noisy image and filtered the noise correspondingly. Almost all these methods [16, 17, 19, 20, 18, 14] use Gaussian or mixture of Gaussians (MoG) to model the noise in real noisy images. However, the noise in real noisy images is very complex and hard to be modeled by explicit distributions.

3. External Prior Guided Internal Prior Learning

In this section, we first describe the learning of external prior, and then describe in detail the guided internal prior learning. Finally, the denoising algorithm with the learned priors is presented.

3.1. Learn External Patch Group Priors

The nonlocal self-similarity based patch group (PG) [7] has proved to be a very effective unit for image prior learning. In this work, we also extract PGs from natural clean images to learn priors. A PG is a group of similar patches to a local patch.

In our method, each local patch is extracted from a

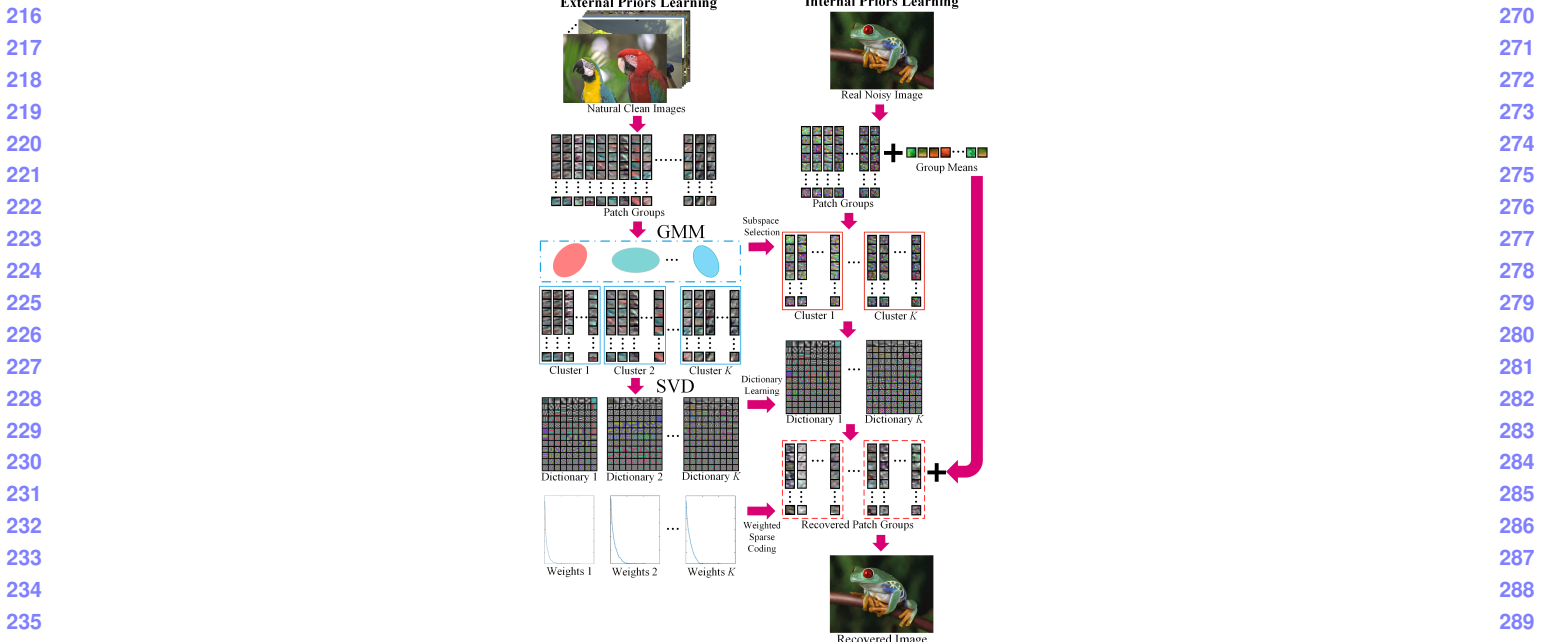


Figure 2. Flowchart of the proposed external prior guided internal prior learning and real noisy image denoising framework.

RGB image with patch size $p \times p \times 3$. We search the M most similar patches to this local patch (including the local patch itself) in a $W \times W$ local region around it. Each patch is stretched to a patch vector $\mathbf{x}_m \in \mathbb{R}^{3p^2 \times 1}$ to form the PG $\{\mathbf{x}_m\}_{m=1}^M$. The mean vector of this PG is $\mu = \frac{1}{M} \sum_{m=1}^M \mathbf{x}_m$, and the group mean subtracted PG is defined as $\bar{\mathbf{X}} \triangleq \{\bar{\mathbf{x}}_m = \mathbf{x}_m - \mu\}$.

Assume we extract a number of N PGs from a set of external natural images, and the n -th PG is $\bar{\mathbf{X}}_n \triangleq \{\bar{\mathbf{x}}_{n,m}\}_{m=1}^M, n = 1, \dots, N$. A Gaussian Mixture Model (GMM) is learned to model the PG prior. The overall log-likelihood function is

$$\ln \mathcal{L} = \sum_{n=1}^N \ln \left(\sum_{k=1}^K \pi_k \prod_{m=1}^M \mathcal{N}(\bar{\mathbf{x}}_{n,m} | \mu_k, \Sigma_k) \right). \quad (1)$$

The learning process is similar to the GMM learning in [7, 13]. Finally, a GMM model with K Gaussian components is learned, and the learned parameters include mixture weights $\{\pi_k\}_{k=1}^K$, mean vectors $\{\mu_k\}_{k=1}^K$, and covariance matrices $\{\Sigma_k\}_{k=1}^K$. Note that the mean vector of each cluster is naturally zero, i.e., $\mu_k = \mathbf{0}$.

To better describe the subspace of each Gaussian component, we perform singular value decomposition (SVD) on the covariance matrix:

$$\Sigma_k = \mathbf{U}_k \mathbf{S}_k \mathbf{U}_k^\top. \quad (2)$$

The eigenvector matrices $\{\mathbf{U}_k\}_{k=1}^K$ will be employed as the external orthogonal dictionary to guide the internal dictionary learning in next sub-section. The singular values in \mathbf{S}_k reflect the significance of the singular vectors in \mathbf{U}_k . They will also be utilized as prior weights for weighted sparse coding in our denoising algorithm.

3.2. Guided Internal Prior Learning

After the external PG prior is learned, we employ it to guide the internal PG prior learning for a given real noisy image. The guidance lies in two aspects. One is that the external prior can guide the subspace assignment of internal noisy PGs, while the other is that the external prior could guide the orthogonal dictionary learning of internal noisy PGs.

3.2.1 Internal Subspace Assignment

Given a real noisy image, we extract N (overlapped) local patches from it. Similar to the external prior learning stage, for the n -th local patch we search its M most similar patches around it to form a noisy PG, denoted by $\mathbf{Y}_n = \{\mathbf{y}_{n,1}, \dots, \mathbf{y}_{n,M}\}$. Then the group mean of \mathbf{Y}_n , denoted by μ_n , is subtracted from each patch by $\bar{\mathbf{y}}_{n,m} = \mathbf{y}_{n,m} - \mu_n$, leading to the mean subtracted noisy PG $\bar{\mathbf{Y}}_n \triangleq \{\bar{\mathbf{y}}_{n,m}\}_{m=1}^M$.

The external GMM prior models $\{\Sigma_k\}_{k=1}^K$ basically characterize the subspaces of natural high quality PGs. Therefore, we project the noisy PG $\bar{\mathbf{Y}}_n$ into the subspaces of $\{\Sigma_k\}_{k=1}^K$ and assign it to the most suitable subspace based on the posterior probability:

$$P(k|\bar{\mathbf{Y}}_n) = \frac{\prod_{m=1}^M \mathcal{N}(\bar{\mathbf{y}}_{n,m} | \mathbf{0}, \Sigma_k)}{\sum_{l=1}^K \prod_{m=1}^M \mathcal{N}(\bar{\mathbf{y}}_{n,m} | \mathbf{0}, \Sigma_l)} \quad (3)$$

for $k = 1, \dots, K$. Then $\bar{\mathbf{Y}}_n$ is assigned to the component with the maximum A-posteriori (MAP) probability $\max_k P(k|\bar{\mathbf{Y}}_n)$.

324
325
326
327
328
329
330
331
332
333
334
335
336
337
338
339
340
341
342

3.2.2 Guided Orthogonal Dictionary Learning

Assume we have assigned all the internal noisy PGs $\{\bar{\mathbf{Y}}_n\}_{n=1}^N$ to their corresponding most suitable subspaces in $\{\mathcal{N}(\mathbf{0}, \Sigma_k)\}_{k=1}^K$. For the k -th subspace, the noisy PGs assigned to it are $\{\bar{\mathbf{Y}}_{k_n}\}_{n=1}^{N_k}$ where $\bar{\mathbf{Y}}_{k_n} = [\bar{\mathbf{y}}_{k_n,1}, \dots, \bar{\mathbf{y}}_{k_n,M}]$ and $\sum_{k=1}^K N_k = N$. We propose to learn an orthogonal dictionary \mathbf{D}_k from each set of PGs $\bar{\mathbf{Y}}_{k_n}$ with the guidance of the corresponding external orthogonal dictionary \mathbf{U}_k (Eq. (2)) to characterize the internal PG prior. The reasons that we learn orthogonal dictionaries are two-fold. Firstly, the PGs $\bar{\mathbf{Y}}_{k_n}$ are in a subspace of the whole space of all PGs, therefore, there is no necessary to learn a redundant over-complete dictionary to characterize it, while an orthonormal dictionary has naturally zero *mutual incoherence* [25]. Secondly, the orthogonality of dictionary can make the encoding in the testing stage very efficient, leading to an efficient denoising algorithm (please refer to sub-section 3.3 for details).

We let the orthogonal dictionary \mathbf{D}_k be $\mathbf{D}_k \triangleq [\mathbf{D}_{k,E} \ \mathbf{D}_{k,I}] \in \mathbb{R}^{3p^2 \times 3p^2}$, where $\mathbf{D}_{k,E} = \mathbf{U}_k(:, 1:r) \in \mathbb{R}^{3p^2 \times r}$ is the external sub-dictionary and it includes the first r most important eigenvectors of \mathbf{U}_k , and the internal sub-dictionary $\mathbf{D}_{k,I}$ is to be adaptively learned from the noisy PGs $\{\bar{\mathbf{Y}}_{k_n}\}_{n=1}^{N_k}$. The rationale to design \mathbf{D}_k as a hybrid dictionary is as follows. The external sub-dictionary $\mathbf{D}_{k,E}$ is pre-trained from external clean data, and it represents the k -th latent subspace of natural images, which is helpful to reconstruct the common latent structures of images. However, $\mathbf{D}_{k,E}$ is general to all images and it is not adaptive to the given noisy image. Some fine-scale details specific to the given image may not be well characterized by $\mathbf{D}_{k,E}$. Therefore, we learn an internal sub-dictionary $\mathbf{D}_{k,I}$ to supplement $\mathbf{D}_{k,E}$. In other words, $\mathbf{D}_{k,I}$ is to reveal the latent subspace adaptive to the input noisy image, which cannot be effectively represented by $\mathbf{D}_{k,E}$.

For notation simplicity, in the following development we ignore the subspace index k for $\bar{\mathbf{Y}}_{k_n}$ and \mathbf{D}_k , etc. The learning of hybrid orthogonal dictionary \mathbf{D} is performed under the following weighted sparse coding framework:

$$\begin{aligned} & \min_{\mathbf{D}_i, \{\alpha_{n,m}\}} \sum_{n=1}^N \sum_{m=1}^M (\|\bar{\mathbf{y}}_{n,m} - \mathbf{D}\alpha_{n,m}\|_2^2 + \sum_{j=1}^{3p^2} \lambda_j |\alpha_{n,m,j}|) \\ & \text{s.t. } \mathbf{D} = [\mathbf{D}_E \ \mathbf{D}_I], \quad \mathbf{D}_I^\top \mathbf{D}_I = \mathbf{I}_r, \quad \mathbf{D}_E^\top \mathbf{D}_I = \mathbf{0}, \end{aligned} \quad (4)$$

where $\alpha_{n,m}$ is the sparse coding vector of the m -th patch $\bar{\mathbf{y}}_{n,m}$ in the n -th PG $\bar{\mathbf{Y}}_n$ and $\alpha_{n,m,j}$ is the j -th element of $\alpha_{n,m}$. λ_j is the j -th regularization parameter defined as

$$\lambda_j = \lambda / (\sqrt{\mathbf{S}_k(j)} + \varepsilon), \quad (5)$$

where $\mathbf{S}_k(j)$ is the j -th singular value of diagonal singular value matrix \mathbf{S}_k (please refer to Eq. (2)) and ε is a small positive number to avoid zero denominator. Noted

that $\mathbf{D}_E = \mathbf{U}_k$ if $r = 3p^2$ and $\mathbf{D}_E = \emptyset$ if $r = 0$. The dictionary $\mathbf{D} = [\mathbf{D}_E \ \mathbf{D}_I]$ is orthogonal by checking that:

$$\mathbf{D}^\top \mathbf{D} = \begin{bmatrix} \mathbf{D}_E^\top \\ \mathbf{D}_I^\top \end{bmatrix} [\mathbf{D}_E \ \mathbf{D}_I] = \begin{bmatrix} \mathbf{D}_E^\top \mathbf{D}_E & \mathbf{D}_E^\top \mathbf{D}_I \\ \mathbf{D}_I^\top \mathbf{D}_E & \mathbf{D}_I^\top \mathbf{D}_I \end{bmatrix} = \mathbf{I} \quad (6)$$

We employ an alternating iterative approach to solve the optimization problem (4). Specifically, we initialize the orthogonal dictionary as $\mathbf{D}^{(0)} = \mathbf{U}_k$ and for $t = 0, 1, \dots, T-1$, we alternatively update $\alpha_{n,m}$ and \mathbf{D} as follows:

Updating Sparse Coefficient: Given the orthogonal dictionary $\mathbf{D}^{(t)}$, we update each sparse coding vector $\alpha_{n,m}$ by solving

$$\alpha_{n,m}^{(t)} := \arg \min_{\alpha_{n,m}} \|\bar{\mathbf{y}}_{n,m} - \mathbf{D}^{(t)} \alpha_{n,m}\|_2^2 + \sum_{j=1}^{3p^2} \lambda_j |\alpha_{n,m,j}| \quad (7)$$

Since dictionary $\mathbf{D}^{(t)}$ is orthogonal, the problems (7) has a closed-form solution

$$\alpha_{n,m}^{(t)} = \text{sgn}((\mathbf{D}^{(t)})^\top \bar{\mathbf{y}}_{n,m}) \odot \max(|(\mathbf{D}^{(t)})^\top \bar{\mathbf{y}}_{n,m}| - \lambda, 0), \quad (8)$$

where $\lambda = [\lambda_1, \lambda_2, \dots, \lambda_{3p^2}]$ is the vector of regularization parameter and $\text{sgn}(\bullet)$ is the sign function, \odot means element-wise multiplication. The detailed derivation of Eq. (8) can be found in the supplementary file.

Updating Internal Sub-dictionary: Given the sparse coding vectors $\alpha_{n,m}^{(t)}$, we update the internal sub-dictionary by solving

$$\begin{aligned} \mathbf{D}_I^{(t+1)} &:= \arg \min_{\mathbf{D}_I} \sum_{n=1}^N \sum_{m=1}^M (\|\bar{\mathbf{y}}_{n,m} - \mathbf{D} \alpha_{n,m}^{(t)}\|_2^2) \\ &= \arg \min_{\mathbf{D}_I} \|\mathbf{Y} - \mathbf{D} \mathbf{A}^{(t)}\|_F^2 \end{aligned} \quad (9)$$

$$\text{s.t. } \mathbf{D} = [\mathbf{D}_E \ \mathbf{D}_I], \quad \mathbf{D}_I^\top \mathbf{D}_I = \mathbf{I}_r, \quad \mathbf{D}_E^\top \mathbf{D}_I = \mathbf{0},$$

where $\mathbf{A}^{(t)} = [\alpha_{1,1}^{(t)}, \dots, \alpha_{1,M}^{(t)}, \dots, \alpha_{N,1}^{(t)}, \dots, \alpha_{N,M}^{(t)}]$. The sparse coefficient matrix can be written as $\mathbf{A}^{(t)} = [(\mathbf{A}_E^{(t)})^\top \ (\mathbf{A}_I^{(t)})^\top]^\top$ where the external part $\mathbf{A}_E^{(t)} \in \mathbb{R}^{(3p^2-r) \times NM}$ and the internal part $\mathbf{A}_I^{(t)} \in \mathbb{R}^{r \times NM}$ represent the coding coefficients of \mathbf{Y} over external sub-dictionary \mathbf{D}_E and internal sub-dictionary \mathbf{D}_I , respectively. According to the Theorem 4 in [26], the problem (9) has a closed-form solution $\mathbf{D}_I^{(t+1)} = \mathbf{U}_i \mathbf{V}_i^\top$, where $\mathbf{U}_i \in \mathbb{R}^{3p^2 \times r}$ and $\mathbf{V}_i \in \mathbb{R}^{r \times r}$ are the orthogonal matrices obtained by the following SVD

$$(\mathbf{I} - \mathbf{D}_E \mathbf{D}_E^\top) \mathbf{Y} (\mathbf{A}_i^{(t)})^\top = \mathbf{U}_i \mathbf{S}_i \mathbf{V}_i^\top. \quad (10)$$

The orthogonality of internal dictionary $\mathbf{D}_i^{(t+1)}$ can be checked by $(\mathbf{D}_i^{(t+1)})^\top (\mathbf{D}_i^{(t+1)}) = \mathbf{V}_i \mathbf{U}_i^\top \mathbf{U}_i \mathbf{V}_i^\top = \mathbf{I}_r$.

3.3. The Denoising Algorithm

The denoising of the given noisy image can be simultaneously done with the guided internal dictionary learning process. Once we obtain the solutions of sparse coding

432 **Alg. 1:** External Prior Guided Internal Prior Learning
 433 for Real Noisy Image Denoising

434 **Input:** Noisy image y , external PG prior GMM model

435 **Output:** The denoised image \hat{x} .

436 **Initialization:** $\hat{x}^{(0)} = y$;

437 **for** $Ite = 1 : IteNum$ **do**

438 1. Extracting internal PGs from $\hat{x}^{(Ite-1)}$;

439 **for** each PG \mathbf{Y}_n **do**

440 2. Calculate group mean vector μ_n and form
 mean subtracted PG $\bar{\mathbf{Y}}_n$;

441 3. Subspace selection via Eq. (3);

442 **end for**

443 **for** the PGs in each Subspace **do**

444 4. External PG prior Guided Internal Orthogonal
 Dictionary Learning by solving (4);

445 5. Recover each patch in all PGs via Eq. (11);

446 **end for**

447 6. Aggregate the recovered PGs of all subspaces to form
 the recovered image $\hat{x}^{(Ite)}$;

448 **end for**

449 vectors $\{\hat{\alpha}_{n,m}^{(T-1)}\}$ in Eq. (8) and the orthogonal dictionary
 450 $\mathbf{D}_{(T)} = [\mathbf{D}_E \mathbf{D}_I^{(T)}]$ in Eq. (9), the latent clean patch of a
 451 noisy patch $\hat{y}_{n,m}$ in PG \mathbf{Y}_n is reconstructed as

$$\hat{y}_{n,m} = \mathbf{D}_{(T)} \hat{\alpha}_{n,m} + \mu_n, \quad (11)$$

452 where μ_n is the group mean of \mathbf{Y}_n . The latent clean image
 453 is then reconstructed by aggregating all the reconstructed
 454 patches in all PGs. We perform the above denoising pro-
 455 cedures for several iterations for better denoising outputs.
 456 The proposed denoising algorithm is summarized in Alg. 1.
 457 The latent clean image \hat{x} is reconstructed by aggregating all
 458 the estimated PGs. Similar to [7], we perform the above de-
 459 noising procedures for several iterations for better denoising
 460 outputs. The proposed denoising algorithm is summarized in
 461 Alg. 1.

4. Experiments

470 We evaluate the performance of the proposed algorithm
 471 on real-world noisy images [14, 20] in comparison with
 472 state-of-the-art denoising methods [5, 6, 9, 8, 10, 11, 14,
 473 19, 20, 21].

4.1. Implementation Details

476 Our proposed method has two stages: the external prior
 477 learning stage and the external prior guided internal prior
 478 learning stage. In the first stage, we set $p = 6$ (the
 479 patch size), $M = 10$ (the number of similar patches in
 480 a PG), $W = 31$ (the window size for PG searching) and
 481 $K = 32$ (the number of Gaussian components in GMM).
 482 We learn the external GMM prior with 3.6 million PGs ex-
 483 tracted from the Kodak PhotoCD Dataset (<http://r0k.us/graphics/kodak/>), which includes 24 high quality
 484 color images.



486
 487
 488
 489
 490
 491
 492
 493
 494
 495
 496
 497
 498
 499
 500
 501
 502
 503
 504
 505
 506
 507
 508
 509
 510
 511
 512
 513
 514
 515
 516
 517
 518
 519
 520
 521
 522
 523
 524
 525
 526
 527
 528
 529
 530
 531
 532
 533
 534
 535
 536
 537
 538
 539

Figure 3. Some samples cropped from real noisy images of [14].

In the second stage, we set $r = 54$ (the number of atoms in the external sub-dictionaries); that is, we let the external sub-dictionary have the same number of atoms as the internal sub-dictionary to be learned. Our experiments show that setting r between 27 and 81 will lead to very similar results. For other parameters, we set $\lambda = 0.001$ (the sparse regularization parameter), $T = 2$ (the number of iterations for solving problem (4)), and $IteNum = 4$ (the number of iterations for Alg.1). All parameters of our method are fixed to all experiments, which are run under the Matlab2014b environment on a machine with Intel(R) Core(TM) i7-5930K CPU of 3.5GHz and 32GB RAM.

4.2. The Testing Datasets

We evaluate the proposed method on two real noisy image datasets, where the images were captured under indoor or outdoor lighting conditions by different types of cameras and camera settings.

The first dataset is provided in [20], which includes 20 real noisy images collected under uncontrolled outdoor environment. Since there is no “ground truth” of the noisy images, the objective measures such as PSNR cannot be computed on this dataset.

The second dataset is provided in [14], which includes noisy images of 17 static scenes. The noisy images were collected under controlled indoor environment. Each scene was shot 500 times under the same camera and camera setting. The mean image of the 500 shots is roughly taken as the “ground truth”, with which the PSNR can be computed. Since the image size is very large (about 7000×5000) and the 17 scenes share repetitive contents, the authors of [14] cropped 15 smaller images (of size 512×512) to perform experiments. To more comprehensively evaluate the proposed methods, we cropped 60 images of size 500×500 from the dataset for experiments. Some samples are shown in Fig. 3. Note that the noise in our cropped 60 images is different from the noise in the 15 images cropped by the authors of [14] since they are from different shots.

4.3. Comparison among external, internal and guided internal priors

To demonstrate the advantages of external prior guided internal priors, in this section we perform real noisy image denoising by using external priors (denoted by “External”), internal priors (denoted by “Internal”), and the proposed guided internal priors (denoted by “Guided Internal”), respectively. For the “External” method, we utilize the full

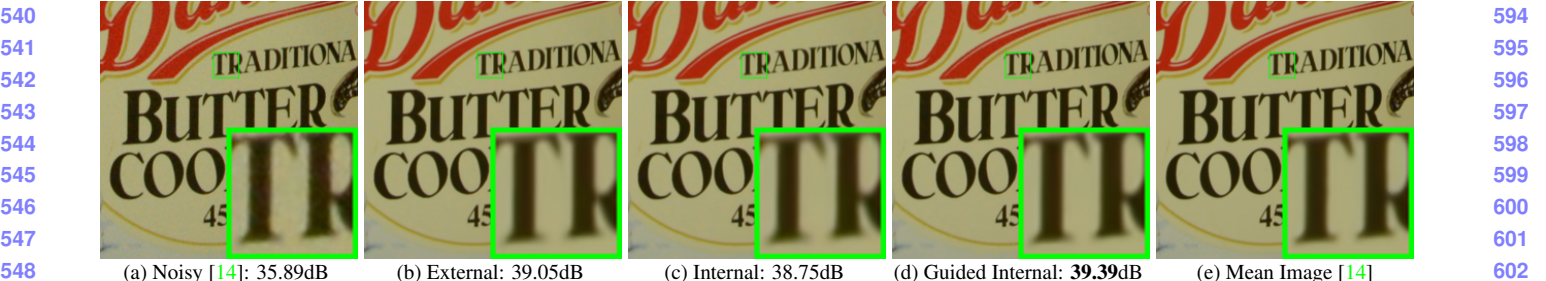


Figure 4. Denoised images of the 96-th cropped image from “Nikon D600 ISO 3200 C1” [14] by different methods. The images are better to be zoomed in on screen.

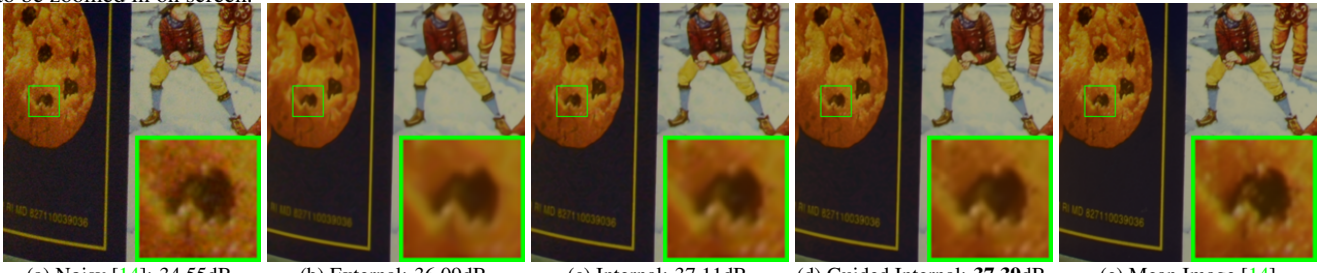


Figure 5. Denoised images of the 94-th cropped image from “Nikon D600 ISO 3200 C1” [14] by different methods. The images are better to be zoomed in on screen.

Table 1. Average PSNR (dB) results and Run Time (seconds) of the External, the Internal, and our proposed methods on 60 real noisy images (of size $500 \times 500 \times 3$) cropped from [14].

	Noisy	External	Internal	Guided Internal
PSNR	34.51	38.21	38.07	38.75
Time	—	39.57	667.36	41.89

external dictionaries (i.e., $r = 108$ in Eq. (4)) for denoising. For the “Internal” method, the overall framework is similar to the method of [3]. A GMM model (with $K = 32$ Gaussians) is directly learned from the PGs extracted from the given noisy image without using any external data, and then the internal orthogonal dictionary is obtained via Eqn. (2) to perform denoising. All parameters of the “External” and “Internal” methods are tuned to achieve their best performance.

We compare the three methods mentioned above on the 60 cropped images from [14]. The average PSNR and run time are listed in Table 1. It can be seen that “Guided Internal” prior achieves better PSNR than both “External” and “Internal” priors. In addition, the “Internal” method is very slow because it involves online GMM learning, while the “Guided Internal” method is only a little slower than the “External” method. Fig. 4 and Fig. 5 show the denoised images of two noisy image by the three methods. We can see that the “External” method is good at recovering large-scale structures (see Fig. 4) while the “Internal” method is good at recovering fine-scale textures (see Fig. 5). By utilizing external priors to guide the internal prior learning, our proposed method can effectively recover both the large-scale structures and fine-scale textures.

4.4. Comparison with State-of-the-Art Denoising Methods

We compare the proposed method with state-of-the-art image denoising methods, including CBM3D [5, 6], WNNM [8], MLP [9], CSF [10], TNRD [11], Noise Clinic (NC) [19], Cross-Channel (CC) [14], and Neat Image (NI) [21]. Among them, CBM3D, WNNM, MLP, CSF and TNRD are designed based on Gaussian noise model, and they need to know the noise level for denoising. We use the method in [27] to estimate the noise level for them. All the other parameters in these methods are set as the default ones. Since WNNM, MLP, CSF and TNRD are designed for grayscale images, we use them to denoise the R, G, B channels separately for color noisy images.

Like our method, the NC is a blind image denoising method which does not need any noise prior. The NI is a commercial software for image denoising, which has been embedded into Photoshop and Corel PaintShop [21]. The code of CC is not released but its results on the 15 cropped images are available at [14]. Therefore, we only compare with it on the 15 cropped images from [14].

4.4.1 Results on Dataset [20]

Since there is no “ground truth” for the real noisy images in dataset [20], we only compare the visual quality of the denoised images by different methods. (Note that method CC [14] is not compared since its code is not available.) Fig. 7 shows the denoised images of “Dog”. It can be seen that CBM3D and WNNM tend to over-smooth much the image while remaining some noise caused color artifacts. MLP

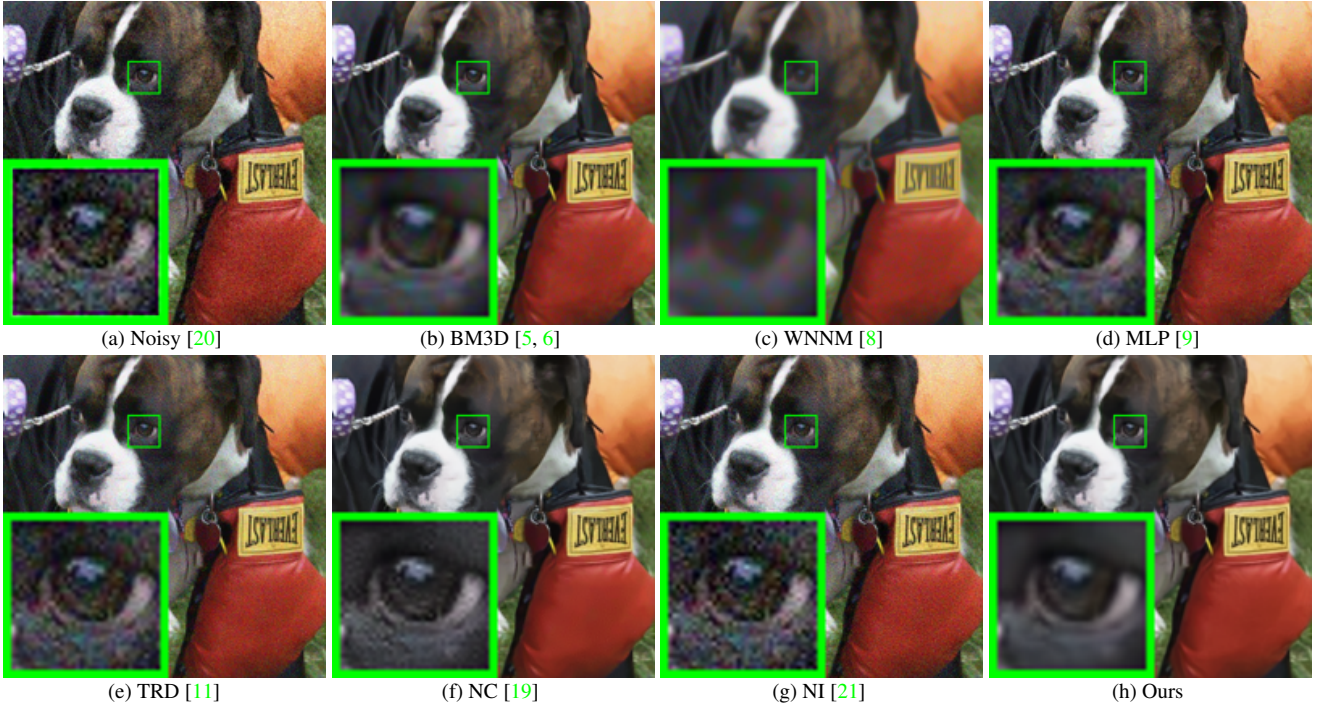


Figure 6. Denoised images of the image “Dog” by different methods. The images are better to be zoomed in on screen.

and TNRD are likely to remain many noise-caused color artifacts across the whole image. These results demonstrate that the methods designed with Gaussian noise model are not effective for real noise removal. Though NC and NI methods are specifically developed for real noisy images, their performance on noise removal is not very satisfactory. In comparison, our proposed method recovers much better the structures and textures (such as the eye area) than the other competing methods. More visual comparisons on dataset [20] can be found in the supplementary file.

4.4.2 Comparison on Dataset [14]

As described in section 4.2, there is a mean image for each of the 17 scenes used in dataset [14], and those mean images can be roughly taken as “ground truth” images for quantitative evaluation of denoising algorithms. We firstly perform quantitative comparison on the 15 cropped images used in [14]. The PSNR results of CBM3D [5], WNNM [8], MLP [9], CSF [10], TNRD [11], NC [19] and CC [14] are listed in Table 3. (The results of CC are copied from the original paper [14].) The best PSNR result of each image is highlighted in bold. One can see that on 9 out of the 15 images, our method achieves the best PSNR values. CC achieves the best PSNR on 3 of the 15 images. It should be noted that in the CC method, a specific model is trained for each camera and camera setting, while our method uses the same model for all images. On average, our proposed method has 0.28dB PSNR improvements over [14] and much higher

Table 2. Average PSNR(dB) results of different methods on 60 real noisy images cropped from [14].

Methods	BM3D	WNNM	MLP	CSF
PSNR	34.58	34.52	36.19	37.40
Methods	TRD	NI	NC	Ours
PSNR	37.75	36.53	37.57	38.75

PSNR gains over other competing methods. Fig. ?? shows the denoised images of a scene captured by Canon 5D Mark 3 at ISO = 3200. We can see that CBM3D, WNNM, NC, NI, and CC would either remain noise or generate artifacts, while MLP, TNRD over-smooth much the image. By using the external prior guided internal priors, our proposed method preserves edges and textures better than other methods, leading to visually pleasant outputs. More visual comparisons can be found in the supplementary file.

We then perform denoising experiments on the 60 images we cropped from [14]. The average PSNR results are listed in Table 2 (CC is not compared since the code of [14] is not available). Again, our proposed method achieves much better PSNR results than the other methods. The improvement of our method over the second best method (TNRD) is about 1dB. Due to the space limitations, the visual comparisons are provided in the supplementary file.

5. Conclusion

The noise in real-world noisy images is much more complex than additive white Gaussian noise and hard to be modeled by simple analytical distributions such as Gaussian or

Table 3. Average PSNR(dB) results of different methods on 15 cropped real noisy images used in [14].

Camera Settings	Noisy	BM3D	WNNM	MLP	CSF	TRD	NI	NC	CC	Ours
Canon 5D Mark III ISO = 3200	37.00	37.08	37.09	33.92	35.68	36.20	37.68	38.76	38.37	40.50
	33.88	33.94	33.93	33.24	34.03	34.35	34.87	35.69	35.37	37.05
	33.83	33.88	33.90	32.37	32.63	33.10	34.77	35.54	34.91	36.11
Nikon D600 ISO = 3200	33.28	33.33	33.34	31.93	31.78	32.28	34.12	35.57	34.98	34.88
	33.77	33.85	33.79	34.15	35.16	35.34	35.36	36.70	35.95	36.31
	34.93	35.02	34.95	37.89	39.98	40.51	38.68	39.28	41.15	39.23
Nikon D800 ISO = 1600	35.47	35.54	35.57	33.77	34.84	35.09	37.34	38.01	37.99	38.40
	35.71	35.79	35.77	35.89	38.42	38.65	38.57	39.05	40.36	40.92
	34.81	34.92	34.95	34.25	35.79	35.85	37.87	38.20	38.30	38.97
Nikon D800 ISO = 3200	33.26	33.34	33.31	37.42	38.36	38.56	36.95	38.07	39.01	38.66
	32.89	32.95	32.96	34.88	35.53	35.76	35.09	35.72	36.75	37.07
	32.91	32.98	32.96	38.54	40.05	40.59	36.91	36.76	39.06	38.52
Nikon D800 ISO = 6400	29.63	29.66	29.71	33.59	34.08	34.25	31.28	33.49	34.61	33.76
	29.97	30.01	29.98	31.55	32.13	32.38	31.38	32.79	33.21	33.43
	29.87	29.90	29.95	31.42	31.52	31.76	31.40	32.86	33.22	33.58
Average	33.41	33.48	33.48	34.32	35.33	35.65	35.49	36.43	36.88	37.16

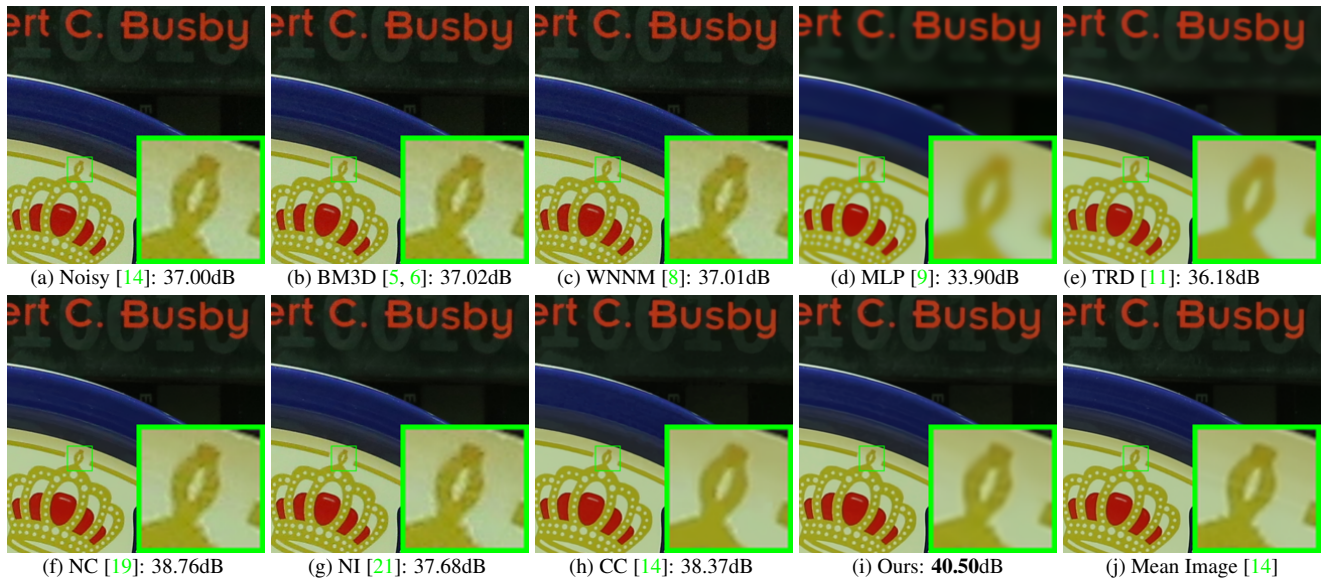


Figure 7. Denoised images of the image “Canon 5D Mark 3 ISO 3200 1” by different methods. The images are better to be zoomed in on screen.

mixture of Gaussians. In this paper, we proposed a simple yet effective solution for real noisy image denoising without explicitly assuming certain noise models. Specifically, we firstly learned image priors of Gaussian Mixture Model from external clean images, and then employ the learned external priors to guide the learning of internal latent priors from the given noisy image. The learned hybrid orthogonal dictionary are simultaneously utilized in real noisy image denoising. Experiments on two real noisy image datasets demonstrate that our proposed method achieved much better performance than state-of-the-art image denoising methods.

References

- [1] M. Elad and M. Aharon. Image denoising via sparse and redundant representations over learned dictionaries. *IEEE Transactions on Image Processing*, 15(12):3736–3745, 2006. 1, 2
- [2] J. Mairal, F. Bach, J. Ponce, G. Sapiro, and A. Zisserman. Non-local sparse models for image restoration. *IEEE International Conference on Computer Vision (ICCV)*, pages 2272–2279, 2009. 1
- [3] W. Dong, L. Zhang, G. Shi, and X. Li. Nonlocally centralized sparse representation for image restoration. *IEEE Transactions on Image Processing*, 22(4):1620–1630, 2013. 1, 2, 6

- 864 [4] A. Buades, B. Coll, and J. M. Morel. A non-local algorithm
865 for image denoising. *IEEE Conference on Computer Vision
866 and Pattern Recognition (CVPR)*, pages 60–65, 2005. 1
- 867 [5] K. Dabov, A. Foi, V. Katkovnik, and K. Egiazarian. Image
868 denoising by sparse 3-D transform-domain collaborative
869 filtering. *IEEE Transactions on Image Processing*,
870 16(8):2080–2095, 2007. 1, 2, 5, 6, 7, 8
- 871 [6] K. Dabov, A. Foi, V. Katkovnik, and K. Egiazarian. Color
872 image denoising via sparse 3D collaborative filtering with
873 grouping constraint in luminance-chrominance space. *IEEE
874 International Conference on Image Processing (ICIP)*, pages
875 313–316, 2007. 1, 2, 5, 6, 7, 8
- 876 [7] J. Xu, L. Zhang, W. Zuo, D. Zhang, and X. Feng. Patch
877 group based nonlocal self-similarity prior learning for image
878 denoising. *IEEE International Conference on Computer Vi-
879 sion (ICCV)*, pages 244–252, 2015. 1, 2, 3, 5
- 880 [8] S. Gu, L. Zhang, W. Zuo, and X. Feng. Weighted nu-
881 clear norm minimization with application to image denoising.
882 *IEEE Conference on Computer Vision and Pattern Recog-
883 nition (CVPR)*, pages 2862–2869, 2014. 1, 2, 5, 6,
884 7, 8
- 885 [9] H. C. Burger, C. J. Schuler, and S. Harmeling. Image de-
886 noising: Can plain neural networks compete with BM3D?
887 *IEEE Conference on Computer Vision and Pattern Recog-
888 nition (CVPR)*, pages 2392–2399, 2012. 1, 2, 5, 6, 7, 8
- 889 [10] U. Schmidt and S. Roth. Shrinkage fields for effective image
890 restoration. *IEEE Conference on Computer Vision and Pat-
891 tern Recognition (CVPR)*, pages 2774–2781, June 2014. 1,
892 2, 5, 6, 7
- 893 [11] Y. Chen, W. Yu, and T. Pock. On learning optimized re-
894 action diffusion processes for effective image restoration.
895 *IEEE Conference on Computer Vision and Pattern Recog-
896 nition (CVPR)*, pages 5261–5269, 2015. 1, 2, 5, 6, 7, 8
- 897 [12] S. Roth and M. J. Black. Fields of experts. *International
898 Journal of Computer Vision*, 82(2):205–229, 2009. 1, 2
- 899 [13] D. Zoran and Y. Weiss. From learning models of natural
900 image patches to whole image restoration. *IEEE Interna-
901 tional Conference on Computer Vision (ICCV)*, pages 479–
902 486, 2011. 1, 2, 3
- 903 [14] S. Nam, Y. Hwang, Y. Matsushita, and S. J. Kim. A holistic
904 approach to cross-channel image noise modeling and its ap-
905 plication to image denoising. *IEEE Conference on Computer
906 Vision and Pattern Recognition (CVPR)*, pages 1683–1691,
907 2016. 1, 2, 5, 6, 7, 8
- 908 [15] G. E Healey and R. Konddepudi. Radiometric CCD cam-
909 era calibration and noise estimation. *IEEE Transactions on
910 Pattern Analysis and Machine Intelligence*, 16(3):267–276,
911 1994. 1
- 912 [16] C. Liu, R. Szeliski, S. Bing Kang, C. L. Zitnick, and W. T.
913 Freeman. Automatic estimation and removal of noise from
914 a single image. *IEEE Transactions on Pattern Analysis and
915 Machine Intelligence*, 30(2):299–314, 2008. 1, 2
- 916 [17] Z. Gong, Z. Shen, and K.-C. Toh. Image restoration with
917 mixed or unknown noises. *Multiscale Modeling & Simula-
918 tion*, 12(2):458–487, 2014. 1, 2